ADVANCES IN ATMOSPHERIC SCIENCES, VOL. 36, SEPTEMBER 2019, 961–974

• **Review** •

# Recent Progress in Dual-Polarization Radar Research and Applications in China

Kun ZHAO*[1,2], Hao HUANG[1,2], Mingjun WANG[1,2], Wen-Chau LEE[3], Gang CHEN[1], Long WEN[1], Jing WEN[1], Guifu ZHANG[1,4], Ming XUE[1,4], Zhengwei YANG[1], Liping LIU[2], Chong WU[2], Zhiqun HU[2], and Sheng CHEN[5]

[1]*Key Laboratory of Mesoscale Severe Weather of Ministry of Education and School of Atmospheric Sciences, Nanjing University, 163 Xianlin Road, Nanjing* 210023*, China*

[2]*State Key Laboratory of Severe Weather and Joint Center for Atmospheric Radar Research of China Meteorological Administration and Nanjing University, Chinese Academy of Meteorological Sciences, Beijing* 100081*, China*

[3]*National Center for Atmospheric Research, Boulder, Colorado* 80301*, USA*

[4]*School of Meteorology and Advanced Radar Research Center, University of Oklahoma, Norman, Oklahoma* 73019*, USA*

[5]*School of Atmospheric Sciences, and Guangdong Province Key Laboratory for Climate Change and Natural Disaster Studies, Sun Yat-sen University, Guangzhou* 510006*, China*

(Received 21 March 2019; revised 7 June 2019; accepted 11 June 2019)

ABSTRACT

Dual-polarization (dual-pol) radar can measure additional parameters that provide more microphysical information of precipitation systems than those provided by conventional Doppler radar. The dual-pol parameters have been successfully utilized to investigate precipitation microphysics and improve radar quantitative precipitation estimation (QPE). The recent progress in dual-pol radar research and applications in China is summarized in four aspects. Firstly, the characteristics of several representative dual-pol radars are reviewed. Various approaches have been developed for radar data quality control, including calibration, attenuation correction, calculation of specific differential phase shift, and identification and removal of non-meteorological echoes. Using dual-pol radar measurements, the microphysical characteristics derived from raindrop size distribution retrieval, hydrometeor classification, and QPE is better understood in China. The limited number of studies in China that have sought to use dual-pol radar data to validate the microphysical parameterization and initialization of numerical models and assimilate dual-pol data into numerical models are summarized. The challenges of applying dual-pol data in numerical models and emerging technologies that may make significant impacts on the field of radar meteorology are discussed.

**Key words**: dual-polarization radar, quantitative precipitation estimation, precipitation microphysics, drop size distribution, numerical model

**Citation**: Zhao, K., and Coauthors, 2019: Recent progress in dual-polarization radar research and applications in China. *Adv. Atmos. Sci.*, **36**(9), 961–974, https://doi.org/10.1007/s00376-019-9057-2.

**Article Highlights**:

- Recent process in dual-pol radar research and applications in China.
- Deeper insights into the precipitation microphysics of severe weather in China.

## 1. Introduction

The first dual-polarization (dual-pol) research radar was developed in the late 1970s in the United States (US) (Seliga and Bringi, 1976, 1978). By adding a vertically (V) polarized channel in addition to the horizontally (H) polarized channel to a conventional radar, dual-pol radars can measure more parameters, including differential reflectivity ($Z_{DR}$), co-polar cross-correlation coefficient ($\rho_{hv}$), differential phase ($\Phi_{DP}$), and specific differential phase ($K_{DP}$), which can provide more microphysical information of precipitation systems (shape, phase, and type of hydrometeors) (e.g., Doviak and Zrnić, 1993; Bringi and Chandrasekar, 2001; Zhang, 2016). In practice, the majority of dual-pol radars transmit in simultaneous H and V mode, for which only the co-polar signals are measured. For several research dual-pol radars, the cross-polar signals can be measured by transmitting alternating H and V modes with two receivers. The US operational radar network, weather surveillance radar (WSR)-88D, completed the upgrade to dual-pol radars in 2013 (Kumjian, 2013). Other regions, including Europe, Canada, Japan, Korea, and China

* Corresponding author: Kun ZHAO
Email: zhaokun@nju.edu.cn

have begun to upgrade their operational radar networks in recent years. The theory behind dual-pol radars and the applications of dual-pol radar data in understanding microphysical processes and quantitative precipitation estimation (QPE) can be found in textbooks (e.g., Doviak and Zrnić, 1993; Bringi and Chandrasekar, 2001; Zhang, 2016) and review articles (e.g., Bluestein et al., 2014; Hubbert et al., 2018; Zhang et al., 2019).

China is one of the countries in the world that suffers severe damage from high-impact weather [e.g., mesoscale convective systems (MCSs), tropical cyclones etc.] and the accompanying flooding and mudslides. To improve the ability in monitoring and nowcasting these high-impact weather events, China has deployed a nationwide radar network since 1999 composed of more than 200 China's New Generation Doppler Weather Radars (CINRAD 98D) in both S- and C-bands. In recent years, with the advent of dual-pol radar technologies in China, several X- and C-band mobile dual-pol radars have been developed by universities and research institutes, including Nanjing University's C-band radar (NJU CPOL) and the Institute of Atmospheric Physics' X-band radar (IAP XPOL). These radars have been used to observe severe weather in field campaigns such as the Observation, Prediction and Analysis of Severe Convection of China (OPACC) (Xue, 2016), the Southern China Monsoon Rainfall Experiment (SCMREX) (Luo et al., 2017), the Understanding and Prediction of Rainfall Associated with Landfalling Tropical Cyclones (UPDRAFT) (Wang, 2018), and the Third Tibetan Plateau Atmospheric Scientific Experiment (TIPEX-III) (Zhao et al., 2018). In 2013, the first operational dual-pol radar (CINRAD 98DP) in China was in service in Zhuhai, Guangdong Province. Since then, more than 10 S-band weather radars in Shanghai City and the provinces of Guangdong, Fujian, and Anhui have been upgraded to dual-pol radars, and more than 100 dual-pol radars will be built or upgraded in China by 2020. To date, the data collected from these dual-pol radars in China have been used and analyzed to improve understanding of precipitation microphysics (e.g., Wang et al., 2016b; Wen et al., 2017) as well as radar QPE and quantitative precipitation forecast (QPF) in China (e.g., Chen et al., 2017; Huang et al., 2018a).

The purpose of this paper is to review the progress and status of dual-pol radars, research results and applications in China, including (1) the characteristics of dual-pol radars and data quality control procedures, (2) rainfall estimation and microphysical retrieval methods from dual-pol radars, (3) precipitation and microphysical characteristics in severe weather deduced from dual-pol radars, and (4) applications of dual-pol radar data in numerical models.

## 2. Characteristics of dual-pol radars and data quality control in China

The characteristics of CINRAD-98D with polarimetric capacity (CIRAD-98DP) and several C- and X-band mobile dual-pol radars in China are summarized in Table 1. Three polarimetric variables are important for radar applications in terms of precipitation and microphysical characteristics: $Z_{DR}$, which is a function of drop shape and a good measure of the median drop diameter; $K_{DP}$, which is more linearly related to rain rate ($R$) than equivalent reflectivity factor at H polarization ($Z_H$) and is immune from radar calibration, attenuation, and partial beam blockage; and $\rho_{hv}$, which is a measure of the diversity of particles (e.g., types, shapes and/or orientations)

**Table 1.** System characteristics of NJU CPOL, CINRAD 98DP, and IAP XPOL.

| Parameter | NJU CPOL | CINRAD 98DP | IAP XPOL |
|---|---|---|---|
| Transmitter | 5.625 GHz (klystron) | 2.90 GHz (klystron) | 9.370 GHz (klystron) |
| PRF | 1000 Hz | 322–1282 Hz | 500–2000 Hz |
| Pulse width | 0.5 μs | 1.57 μs | 0.5 μs/1 μs/2 μs |
| Peak power | > 250 kW | 700 kw | 80 kW |
| Antenna gain | > 41 dB | 44.7 dB | 44.78 dB |
| Antenna aperture | 3.2 m | 8.5 m | 2.4 m |
| Beam width | 1.2° | 0.95° | 1° |
| Polarimetric mode | STSR† and LDR mode‡ | STSR | STSR |
| Scan mode | PPI and RHI | PPI | PPI and RHI |
| Radial resolution | 75 m | 250 m | 75 m/150 m/300 m |
| Radar variables | $Z_H$, $Z_{DR}$, $\Phi_{DP}$, $\rho_{hv}$, $L_{DR}$, $v_r$, $\sigma_v$§ | $Z_H$, $Z_{DR}$, $\Phi_{DP}$, $\rho_{hv}$, SNR, $v_r$, $\sigma_v$ | $Z_H$, $Z_{DR}$, $\Phi_{DP}$, $\rho_{hv}$, SNR, $v_r$, $\sigma_v$ |
| $Z_H$ precision | 1.0 dB | 1.0 dB | 1.0 dB |
| $v_r$ precision | 1 m s$^{-1}$ | 1 m s$^{-1}$ | 1 m s$^{-1}$ |
| $\sigma_v$ precision | 1.0 m s$^{-1}$ | 1.0 m s$^{-1}$ | 1.0 m s$^{-1}$ |
| $Z_{DR}$ precision | 0.2 dB | 0.2 dB | 0.2 dB |
| $\Phi_{DP}$ precision | 2.0° | 2.0° | 2.0° |
| Field campaigns | OPACC UPDRAFT SCMREX | UPDRAFT SCMREX | OPACC |

†STSR: simultaneous transmitting and simultaneous receiving.
‡LDR mode: only transmitting signal at horizontal polarization and receiving at signals at both horizontal and vertical polarizations, in which the linear depolarization ratio can be measured.
§$L_{DR}$, $v_r$, and $\sigma_v$ represent linear depolarization ratio, radial velocity and velocity spectrum.

within a radar sampling volume. Meteorological targets typically possess $\rho_{hv} > 0.8$, where $\rho_{hv}$ for pure rain and snow is close to 1.

For QPE or hydrometeor classification (HC), the desired accuracies for $Z_H$ and $Z_{DR}$ are 1 dB and 0.1–0.2 dB, respectively (Bringi and Chandrasekar, 2001; Chandrasekar et al., 2015). Common procedures to calibrate $Z_H$ and $Z_{DR}$ include using a test signal, sun scans, and backscatter signal from a metallic sphere (Hubbert et al., 2003; Ryzhkov et al., 2005b; Zrnic et al., 2006). $Z_{DR}$ can also be calibrated using signals from drizzle and dry aggregated snow (Ryzhkov et al., 2005b). The accuracy of $Z_H$ can also be benchmarked against the values calculated from $Z_{DR}$ and $K_{DP}$ according to the self-consistency of radar variables (Gorgucci et al., 1992; Vivekanandan et al., 2003). These methods have been widely utilized in recent studies in China (Du et al., 2012, 2013; Hu et al., 2014; Huang et al., 2017). Generally, different $Z_{DR}$ calibration methods result in similar results. However, the quality of rotary joints can degrade over time and use, and influence the consistency of the dual channels of dual-pol radars. Thus, the bias of $Z_{DR}$ can vary with azimuth, which should also be considered in $Z_{DR}$ calibration (Chen et al., 2018; Hu et al., 2018).

S-band dual-pol radars are less subject to attenuation in heavy rainfall and are primarily used for the national weather surveillance radar network in China, similar to those used in the US. However, X- and C-band dual-pol radars are also widely used in China (e.g., citywide radar networks and research radars), which require attenuation correction for quantitative or even qualitative applications when using algorithms developed for S-band radars (Carey et al., 2000). $\Phi_{DP}$ and $K_{DP}$ are mostly unaffected by attenuation despite it being able to reduce the signal-to-noise ratio (SNR) and degrade the quality of $\Phi_{DP}$. $\Phi_{DP}$ can be utilized to improve the accuracy of attenuation correction (Bringi and Chandrasekar, 2001). Two approaches for attenuation correction are commonly used in China: (1) specific attenuation ($A_H$) and specific differential attenuation ($A_{DP}$) are linearly related to $K_{DP}$ (Bringi et al., 1990; Lei, 2014; Wu and Huang, 2014; Huang et al., 2018b), and (2) the "ZPHI" rain-profiling algorithm, where $A_H$ is derived from attenuated reflectivity factor under the constraints of total path-integrated attenuation (Testud et al., 2000). To mitigate the impacts of raindrop size distribution (DSD) variabilities, the ratio $\alpha$ used in the ZPHI algorithm can be adaptively adjusted using the self-consistency of polarimetric variables.

$K_{DP}$ is widely utilized in QPE because the relationship between $K_{DP}$ and $R$ is less affected by the DSD variabilities than $Z$–$R$ relationships (Bringi and Chandrasekar, 2001). However, $K_{DP}$ is not directly measured; instead, it is estimated from the range derivative of filtered $\Phi_{DP}$ (Hubbert et al., 1993; Hubbert and Bringi, 1995) to avoid random errors in $\Phi_{DP}$ propagating to $K_{DP}$ and producing erroneous negative values for rain or for rain mixtures. Thus, $\Phi_{DP}$ is usually first processed/filtered using running average method (Wei et al., 2014), median average method (Wei et al., 2014; Wu et al., 2017), finite-impulse response filter (Hubbert et al., 1993; Hubbert and Bringi, 1995), Kalman filter (Wang and Chandrasekar, 2009), wavelet analysis (Hu and Liu, 2014), or the linear fitting and recurrence method (Sun et al., 2015). Huang et al. (2017) proposed a hybrid method by combining the physical constraints of $K_{DP}$ (calculated from $Z_H$ and $Z_{DR}$ using self-consistent relationship, Vivekanandan et al., 2013) and the linear programming algorithm (Giangrande et al., 2013) to improve the estimates of $K_{DP}$ and rainfall.

## 3. Precipitation characteristics retrieved from dual-pol radars

### 3.1. *Hydrometeor Classification*

Dual-pol radar is capable of identifying the primary hydrometeor type in a radar sampling volume because hydrometeor size, shape, orientation, phase, and bulk density affect dual-pol radar observables to different degrees. The relationships between the distributions of dual-pol radar measurements and the hydrometeor types overlap and are not well defined. Therefore, a fuzzy logic approach, which assigns membership functions for each radar observable to account for the overlapping and soft boundaries, has been widely used in HC for both research and operations (Vivekanandan et al., 1999; Park et al., 2009; Dolan et al., 2013). These membership functions should be tuned for different weather regimes, geographical regions, and type of radars. In China, most HC studies adjusted the membership functions of existing methods, (e.g., Park et al., 2009), for different regions (Wu et al., 2018a) and different radar frequencies (Gu et al., 2015; Ran et al., 2017; Feng et al., 2018). In Wu et al. (2018a), the method of Park et al. (2009) was used for radars in South China. Due to the differences in polarimetric characteristics of some hydrometeors between China and the US, applying US HC membership functions in South China results in insufficient discrimination of aggregate values. Discontinuities are found in hail, graupel, wet snow, and heavy rainfall areas (within the dotted line in Fig. 1b). By tuning (statistics-based optimization) the membership functions, the HC results in Fig. 1c are more coherent.

Considering the limitation of the fuzzy logic–based HC method, statistical decision theories, e.g., the maximum likelihood and Bayesian theory, have also been applied for HC in China in recent years (Marzano et al., 2008), where the hydrometeor types are determined using a posteriori probability. The statistical information can also be used to constrain HC by using the a priori distribution. In the work of Wen et al. (2015) and Wen et al. (2016), the conditional probability distribution of the polarimetric variables and ambient temperature corresponding to different hydrometeor types were derived by applying clustering techniques, and were successfully used for the HC of hailstorms and shallow Arctic mixed-phase clouds. Yang et al. (2017) recently proposed a Bayesian-based HC algorithm, in which the conditional probability functions of polarimetric variables are constructed for seven different hydrometeor types. Since the method is statistically trained using radar observations in China, it has been

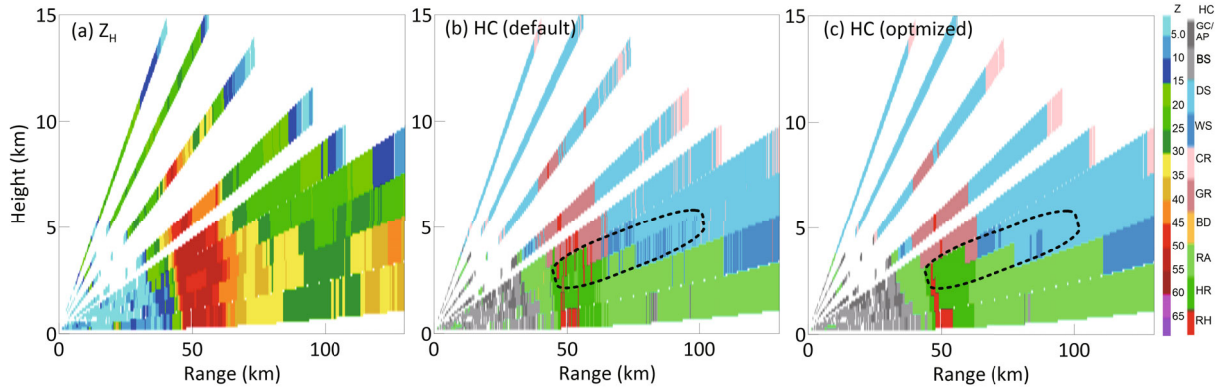


**Fig. 1.** Vertical structure of a squall line in South China observed by Zhuhai dual-pol radar, 10 May 2014: (a) horizontal reflectivity; (b) HC based on fuzzy logic; (c) optimized HC. The colors in (b, c) represent different classes of scatterers, including ground clutter or anomalous propagation, biological scatterers, dry snow, wet snow, crystal, graupel, big drops, rain, moderate light and moderate rain, heavy rain, and hail or the mixture of rain and hail.

proven to produce more reasonable hydrometeor types than the fuzzy logic method for a squall line event that occurred on 30 July 2014 in eastern China. It could be a promising way to achieve HC for dual-pol radar measurements.

### 3.2. *QPE*

Many dual-pol radar rainfall estimators have been developed, including $R(Z_H, Z_{DR})$, $R(K_{DP})$, and $R(K_{DP}, Z_{DR})$ (Ryzhkov and Zrnić, 1995; Gorgucci et al., 2001; Ryzhkov et al., 2005a; Lee, 2006; Bringi et al., 2011), and they have yielded better rainfall estimation than the conventional $Z$–$R$ relation, $R(Z_H)$, particularly for moderate and heavy rain. Dual-pol radar rainfall estimators mainly suffer from uncertainty in two aspects: the model errors caused by DSD variabilities and the measurement errors. To make rainfall estimators more consistent with microphysical climatology in China, DSDs derived from disdrometers have been used to tune dual-pol radar rainfall estimators, and these estimators have been widely applied and evaluated in China (Gao et al., 2014; Zheng et al., 2014; Wei et al., 2016; Chen et al., 2017; Zhang et al., 2017c). Among them, $R(K_{DP})$ provided the best rainfall estimation for X- and C-band radars that are susceptible to severe attenuation in heavy precipitation (Wei et al., 2016; Chen et al., 2017).

For light rain, the advantage of polarimetric rainfall estimators over the conventional $Z$–$R$ relationship diminishes, because measurement errors carry a greater weight than the useful information contained in $Z_{DR}$ and $K_{DP}$. To improve rainfall estimation, Chen et al. (2017) proposed a new composite rainfall estimator, $R(Z_H, K_{DP}, Z_{DR})$, which is constructed by combining $R(Z_H)$, $R(Z_H, Z_{DR})$ and $R(K_{DP})$, based on the statistical QPE error in the $Z_H$–$Z_{DR}$ space, and was proven to outperform any single rainfall estimator in typical heavy rainfall events (e.g., mei-yu, typhoon rainbands and squall lines) in East China. However, the composite estimator is sometimes discontinuous owing to the hard thresholds for switching among different rainfall estimators. To overcome this drawback, Huang et al. (2018a) proposed using a variational approach for QPE, which statistically combines the information provided by radar measurements ($Z_H$ and $\Phi_{DP}$) and applies spatial continuity of rainfall in a unified framework. In this method, the $R$–$K_{DP}$ relationship, tuned using DSD observations in South China, is used for the construction of the forward operator; the tuned $R(Z_H)$ is used as the *a priori*, with its error covariance matrix statistically determined, which can help to reduce the effect of measurement errors in $\Phi_{DP}$. It is found that the variational approach produces better rainfall estimation than the traditional rainfall estimator $R(K_{DP})$ or composite algorithm in multiple rainfall cases, showing higher correlation coefficients and lower normalized absolute errors (Fig. 2).

### 3.3. *Retrieval of DSD*

DSD is a fundamental characteristic of rain microphysics, which can be used to represent all rain physical parameters. Since a DSD contains numerous unknowns, the exponential distribution (Blanchard, 1953; Seliga and Bringi, 1978) and the gamma distribution (Ulbrich, 1983) have been proposed to approximate natural DSDs. It is well-known that retrieving DSDs from polarimetric data using a three-parameter gamma distribution is ill-posed (e.g., Huang et al., 2019). An extra physical constraint for the gamma distribution model, e.g., the statistical relation between the parameters $\mu$ and $\Lambda$ (the slope term) or a fixed value for $\mu$, helps to improve the accuracy of DSD retrieval from $Z_H$ and $Z_{DR}$ (Seliga and Bringi, 1978; Zhang et al., 2001). As revealed by the result in Huang et al. (2019) (Fig. 3), when the $\mu$ and $\Lambda$ relation is utilized in the retrieval, the radar-derived precipitation parameters ($R$, mass-weighted mean diameter $D_m$, and total number concentration $N_t$) are generally consistent with the measurements from disdrometers; when a three-parameter gamma distribution is used as the model for DSD retrieval, the correlation coefficients of $R$, $D_m$ and $N_t$ between the estimates and measurements decrease to 0.58, 0.48 and 0.04 (not shown), respectively. Since DSDs can vary with different climate regions and different geophysical locations, $\mu$–$\Lambda$ relationships need to be refined in different locations of China. Li et al. (2015), Wen et al. (2018) and Liu et al. (2018) have con-

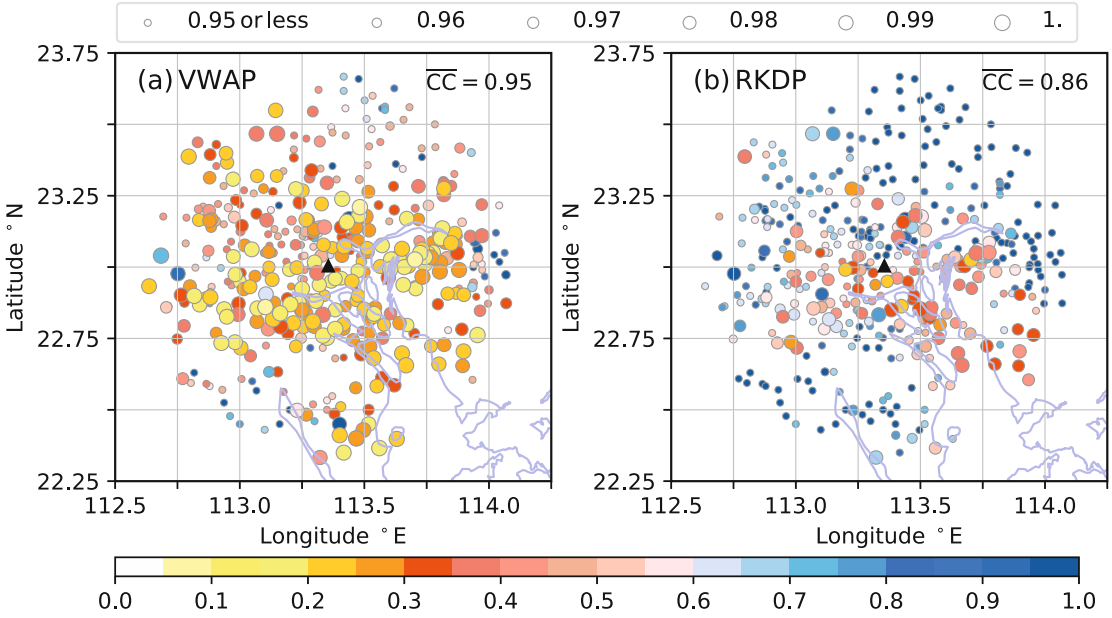


**Fig. 2.** Hourly rainfall comparisons at rain gauge sites for (a) the variational approach of Huang et al. (2018a) with $R(Z_H)$ as the a priori and (b) the conventional $K_{DP}$-based approach. The places where the rain gauges were deployed are shown as circles, wherein the size of the circles represents the correlation coefficient between the time series of the radar-derived accumulated rainfalls (AR) and the time series of the gauge-derived AR, and the color represents the normalized absolute error (NE) between them. The NE is defined as $\mathrm{NE} = \frac{1}{N}\sum_{i=1}^{N}|R_e(i) - R_g(i)|/\overline{R_g}$, where $N$ is the total sampling number at each gauge site, $R_g(R_e)$ is the hourly rainfall from gauge measurements (radar estimation), and $\overline{R_g}$ is the corresponding mean value. [Reprinted from Huang et al. (2018a). © American Meteorological Society. Used with permission.]

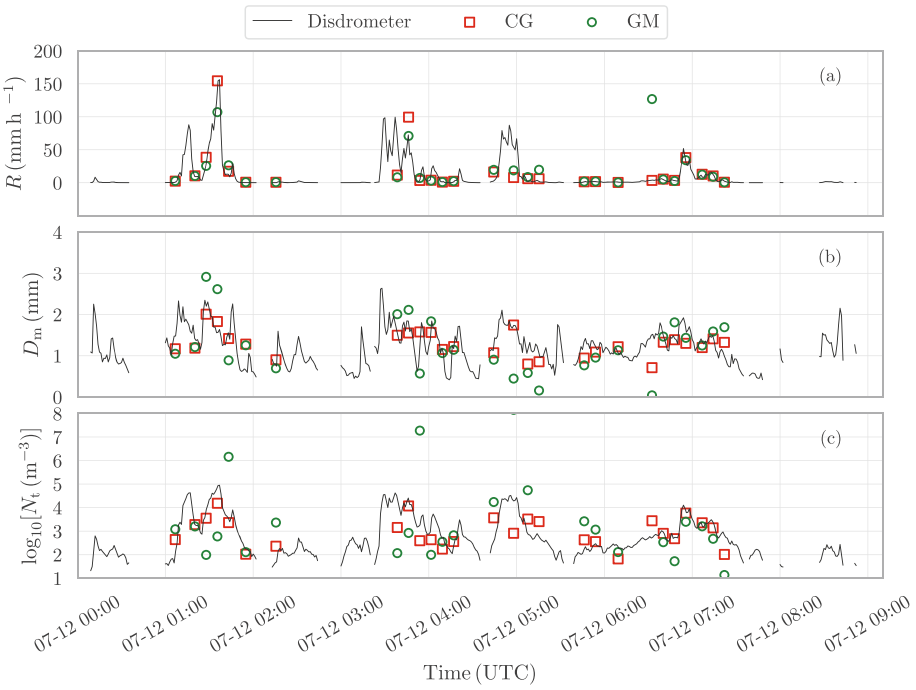


**Fig. 3.** Comparisons of radar-retrieved (a) $R$, (b) $D_m$, and (c) total number concentration $N_t$ with those calculated from 2DVD data (black lines). The red dots and green circles represent the results from error minimization analysis (EMA)-based retrieval using a constrained-gamma distribution (CG) and the three-parameter gamma distribution (GM) with $K_{DP}$ measurements included. [Reprinted from Huang et al. (2019). © American Meteorological Society. Used with permission.]

structed and applied $\mu$–$\Lambda$ relationships to DSD retrievals in Northeast, East and South China, respectively.

To reduce the impact of measurement errors on the retrievals, Huang (2018) proposed using variational analysis for DSD retrieval. In this optimization, the attenuation effects are considered in observation operators, which help to avoid the error propagation from attenuation correction to DSD retrieval. The measurement errors are also mitigated by an azimuthal Kalman filter and a radial B-spline filter. Verification using C- and S-band radar observations shows satisfactory performance of the variational approach.

## 4. Precipitation microphysics and processes in China revealed by dual-pol radar

Precipitation microphysics is one of the key factors determining the behaviors of convective systems owing to the nonlinear interactions between microphysics and dynamics through latent heat release or absorption in microphysical processes. The 3D predominant hydrometeor and DSD distribution can be obtained by using HC algorithms and DSD retrieval methods, as described in section 3, to portray microphysical characteristics with high temporal and spatial resolution and infer the dominant microphysical process (Kumjian and Ryzhkov, 2010, 2012; Kumjian and Prat, 2014; Barnes and Houze, 2016; Wang et al., 2018b).

DSDs of convective rain in different climatic regimes exhibit two clusters within the framework of generalized intercept and median volume diameter, known as the so-called "maritime-like" and "continental-like" DSD characteristics (Bringi et al., 2003). In general, maritime-type convective precipitation possesses a higher number concentration of small/medium sized raindrops than continental-type convective precipitation. Recently, Dolan et al. (2018) revealed that the variation of environmental conditions, in addition to geographic locations, also affects the microphysical properties of convective systems, based on twelve sets of disdrometer observations across three latitudinal bands across the globe. Over the past five years, precipitation microphysics has been investigated extensively in different convective systems in China by combining dual-pol radar observations and disdrometer observations or numerical model results.

### 4.1. *Polarimetric signatures and precipitation microphysics in convective systems*

The microphysical characteristics of MCSs in the US have been well documented, especially for supercell thunderstorms. Typical polarimetric signatures in supercells were reviewed and summarized by Kumjian and Ryzhkov (2008), including the $Z_{DR}$ arc, $K_{DP}$ foot, $Z_{DR}$ column/ring, $K_{DP}$ column, $\rho_{hv}$ ring, large hail signature, and so on.

Similar signatures have also been observed in different convective systems in China, such as hailstorms (Chen et al., 2014), supercell storms (Zhang et al., 2017a), and MCSs (Zhang et al., 2017b). A supercell case that occurred in Qingyuan was studied by Zhang et al. (2017a) using data collected by an S-band dual-pol radar. In that case, a similar large hail signature was presented as large $Z_H$, reduced $\rho_{hv}$, and near-zero $Z_{DR}$. Wang et al. (2018a) presented a $Z_{DR}$ column within updrafts and $Z_{DR}$ arc near the forward-flank downdraft from a supercell (Fig. 4). Zhang et al. (2018) used an X-band dual-pol radar to identify the tornadic debris signature from the Foshan tornado within an outer rainband of Typhoon Mujigae.

Based on dual-pol radar observations from OPACC, SCMREX and TIPEX-III, microphysical processes in different regions of China have been investigated (e.g., Gao et al., 2016; Luo et al., 2017; Wen et al., 2017; Wang et al., 2019). Wen et al. (2017) investigated the variations of microphysical characteristics within the convective region during the formative, intensifying, and mature stages of a subtropical squall line in summer using the NJU-CPOL observations during OPACC in eastern China. The radar-derived DSD in the convection region of a squall line evolved from more continental-like to maritime-like characteristics when the system developed from the formative stage to the mature stage (Fig. 5), which is different from previous studies where the DSD characteristics of a convective line mostly depend on the geographical location rather than within the life cycle of a squall line (Petersen and Rutledge, 2001). The dual-pol radar–derived liquid water content below the freezing level in the convective region was three times higher than the ice water content above the freezing level, indicating the dominance of the warm rain process within this squall line. Luo et al. (2017) showed RHI scans of two MCSs over Guangdong collected by a C-band dual-pol radar in the SCMREX field campaign (Fig. 6). $Z_{DR}$ and $K_{DP}$ columns were identified within convective regions, indicating vigorous updrafts. The increases of $Z_H$, $Z_{DR}$ and $K_{DP}$ toward the ground provided clear signatures of rainwater growth through warm-rain processes. Raindrop breakup was also noticed below the altitude of 2 km, which was characterized as $K_{DP}$ and $Z_{DR}$ decreasing toward the ground. Contrary to MCSs in East and South China where warm-rain processes are dominant owing to the influence of the East Asian summer monsoon, MCSs over the Tibetan Plateau develop much deeper with more distinct ice processes (Mei et al., 2018).

### 4.2. *Precipitation microphysics of landfall typhoons*

In China, the DSDs of landfalling TCs observed by 2-dimensional video disdrometers (2DVDs) mainly consist of very small drops and high number concentrations—more like maritime-type convection than those of TCs in Taiwan (Chang et al., 2009; Wen et al., 2018). The DSDs in the inner rainband of Typhoon Matmo (2014) observed by a 2DVD and retrieved from dual-pol radar measurements also show the characteristics of typical maritime-type convection (Fig.7) (Wang et al., 2016b; Wen et al., 2018). It is also found that warm-rain processes were predominant within the convective region of the inner rainband of Typhoon Matmo (2014).

Based on HC, Wang et al. (2018b) further found that heavy rainfall tends to locate in the updraft and downdraft regions affected by graupel. Within the updraft region, heavy

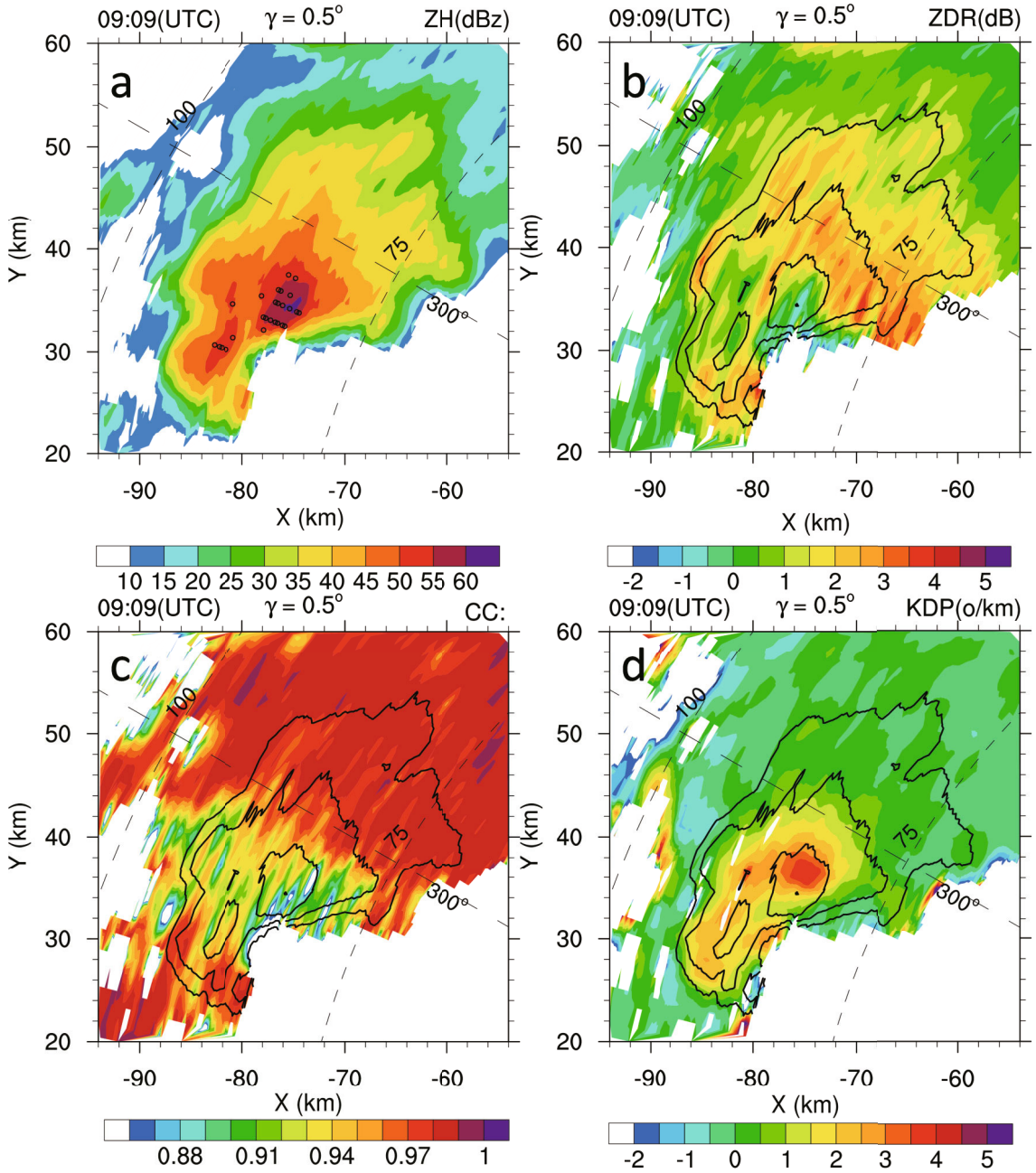


**Fig. 4.** PPI of Zhuhai S-band dual-pol radar at 0.5° elevation at 0909 UTC 20 April 2015: (a) $Z_H$; (b) $Z_{DR}$; (c) $\rho_{hv}$; (d) $K_{DP}$. [Reprinted from Wang et al. (2018a)]

rainfall was generally produced by the warm-rain processes of auto-conversion, accretion, and coalescence from 5 km to 0.5 km in altitude, while melting of graupel particles dominated in the downdraft region.

Wu et al. (2018b) examined the microphysics of convective cells in an outer rainband of Typhoon Nida (2016) using an S-band dual-pol radar. Combining $Z_H$, $Z_{DR}$ and $K_{DP}$ information suggested a layered microphysical structure with riming near the −5°C level, aggregation around the −15°C level, and deposition almost everywhere above the freezing level. Ice processes dominated the precipitation in outer rainbands, being characterized by a much higher $Z_H$ and $Z_{DR}$ (Fig. 8).

## 5. Use of dual-pol radar data for nowcasting and NWPs

Dual-pol radar observations have been used to validate numerical model outputs using forward operators (Vivekanandan et al., 1991; Ryzhkov et al., 2011), as well as parameterize and initialize numerical models by radar data assimilation (e.g., Jung et al., 2008; Posselt et al., 2015). As more dual-pol data have become available from several field experiments in China, these data have provided unique opportunities to validate numerical model results (Gao et al., 2016; Wang et al., 2016a; Wen, 2017). Wang et al. (2016a) developed a simulator to transfer model outputs into S-band

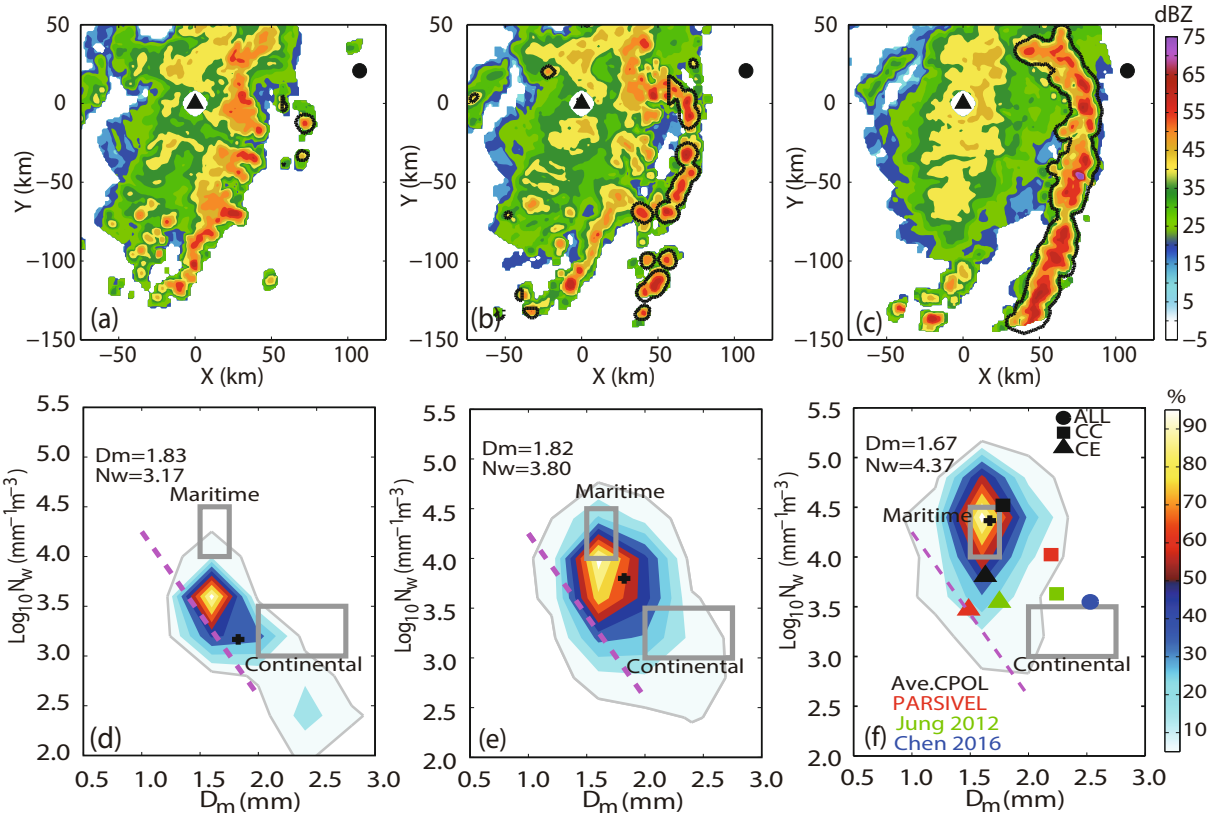


**Fig. 5.** (a–c) The CAPPI of $Z$ km above ground level from the NJU C-POL radar at 2157 LST (formative stage), 2217 LST (developing stage), and 2251 LST (mature stage), respectively, 30 July 2014. The convective region is enclosed by the black solid lines. (d, e) Frequency distribution of $D_m$ and lg$N_w$ retrieved using the constrained-gamma model from the C-POL radar data of convective regions, at 1-km elevation only, for the three stages (a–c). The outermost gray line represents 5% contours. The mean $N_w$ and $D_m$ values for all convective regions are represented by the black plus signs. The two gray rectangles correspond to the maritime and continental convective clusters reported by Bringi et al. (2003). In (f), the square signs represent mean values for the convective center (CC), and the triangle signs represent those for the convective edge (CE) combined. [Reprinted from Wen et al. (2017).]

dual-polar radar parameters based on Rayleigh–Gans scattering theory. The simulator can calculate polarimetric variables by using cloud mixing ratios and number concentrations from microphysics schemes and the axis ratio, relative dielectric constant and canting angles of particles. It can reproduce typical polarimetric radar signatures of a mature 2D idealized squall line, including hail with high $Z_H$ and low $Z_{DR}$, and a $Z_{DR}$ column in the convective updraft region. Gao et al. (2016) found that $Z_{DR}$ was higher (lower) in the convective (stratiform) regions compared to observations for a plateau summertime rainfall event, and thus identified bias in modeled hydrometeor types. Recently, Wen (2017) simulated a squall line system using the ARPS model with three bulk schemes. They found that microphysics schemes with different moments had large impacts on the simulated polarimetric radar variables, and the three-moment scheme reproduced the best characteristics of the simulated squall line.

These limited number of studies focused mainly on summertime convective systems and compared simulations to dual-pol radar observations. As more dual-pol CINRAD-98Ds become available in the future, there will be more opportunities in China for model comparisons, forecast evaluations, and radar data assimilation.

## 6. Summary and future outlook

This paper has reviewed recent advancements in dual-pol radar in China, including radar data quality control, microphysical retrieval algorithms and microphysical characteristics of summer precipitation systems, to guide efforts to further utilize dual-pol radars in the understanding, warning and forecasting severe weather. Studies indicate the importance of environmental conditions rather than latitude-dependence in determining the dominant microphysical processes and DSDs suggested in Dolan et al. (2018). The limited number of studies in China that have sought to use dual-pol radar data to validate the microphysical parameterization and initialization of numerical models and assimilate dual-pol data into numerical models have been summarized. This line of work remains a ongoing research topic, and thus the research community will face many technical challenges in the foreseeable future.

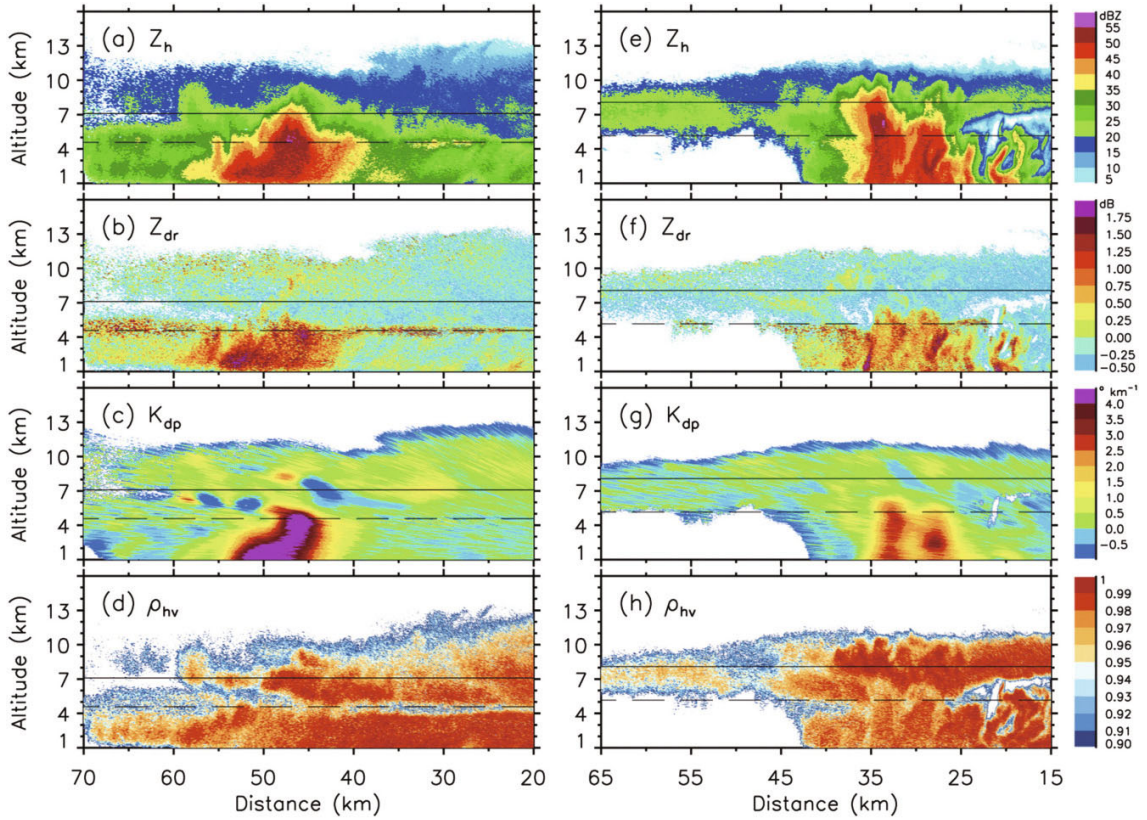


**Fig. 6.** Vertical cross section at about 1752 Local Standard Time (LST) 8 May 2014 of the Heshan C-POL measurements of (a) reflectivity $Z_H$, (b) differential reflectivity $Z_{DR}$, (c) specific differential phase $K_{DP}$, and (d) correlation coefficient $\rho_{hv}$. The black dashed and solid lines represent the 0°C level (4.6 km) and −15°C level (7 km), respectively, according to sounding data. (e–h) As in (a–d), respectively, but at about 1604 LST 22 May 2014; the 0°C and −15°C levels are 5.2 and 8.1 km, respectively. [Reprinted from Luo et al. (2017). © American Meteorological Society. Used with permission.]

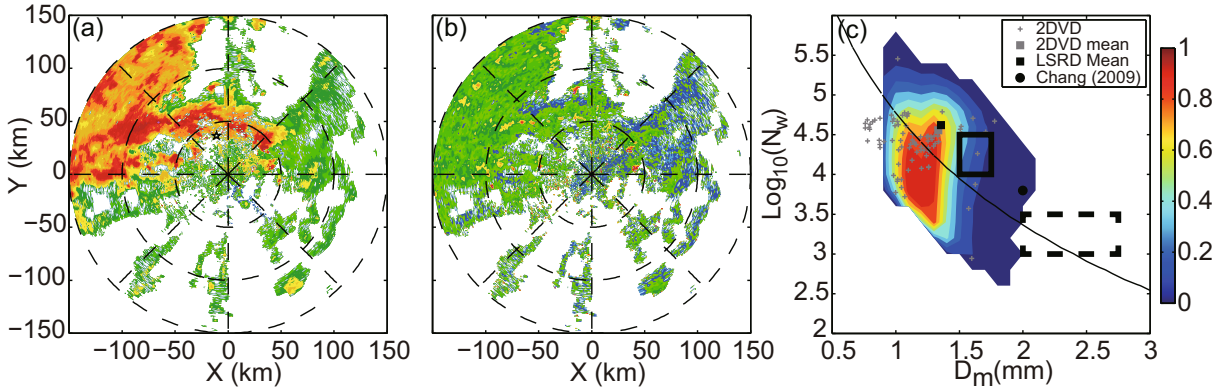


**Fig. 7.** The (a) reflectivity and (b) differential reflectivity at 0.5° elevation observed by Lishui Radar (LSRD) at 1100 UTC 24 September 2014. (c) Frequency of occurrences (color shaded) of $D_m$ (units: mm) and logarithmic $N_w$ (units: mm$^{-1}$ m$^{-3}$) of the retrieved DSDs from LSRD. The gray crosses represent the $D_m$ and $N_w$ values calculated from 2DVD data. The dashed line indicates the rainfall rate of 10 mm h$^{-1}$. The two outlined solid/dashed squares represent the maritime/continental types of convective systems. The gray square, black square, and black dot indicate the mean value of $D_m$ and $N_w$ from 2DVD, LSRD, and the study of Chang et al. (2009) for rainfall rates over 10 mm h$^{-1}$. [Reprinted from Wang et al. (2016b).]

Microphysical parameterization is very important for numerical weather models to accurately simulate precipitation systems. To improve parameterization schemes, efforts are still needed to gain knowledge of precipitation microphysics using different types of instruments, especially dual-pol radars, in the future. In addition, developing techniques

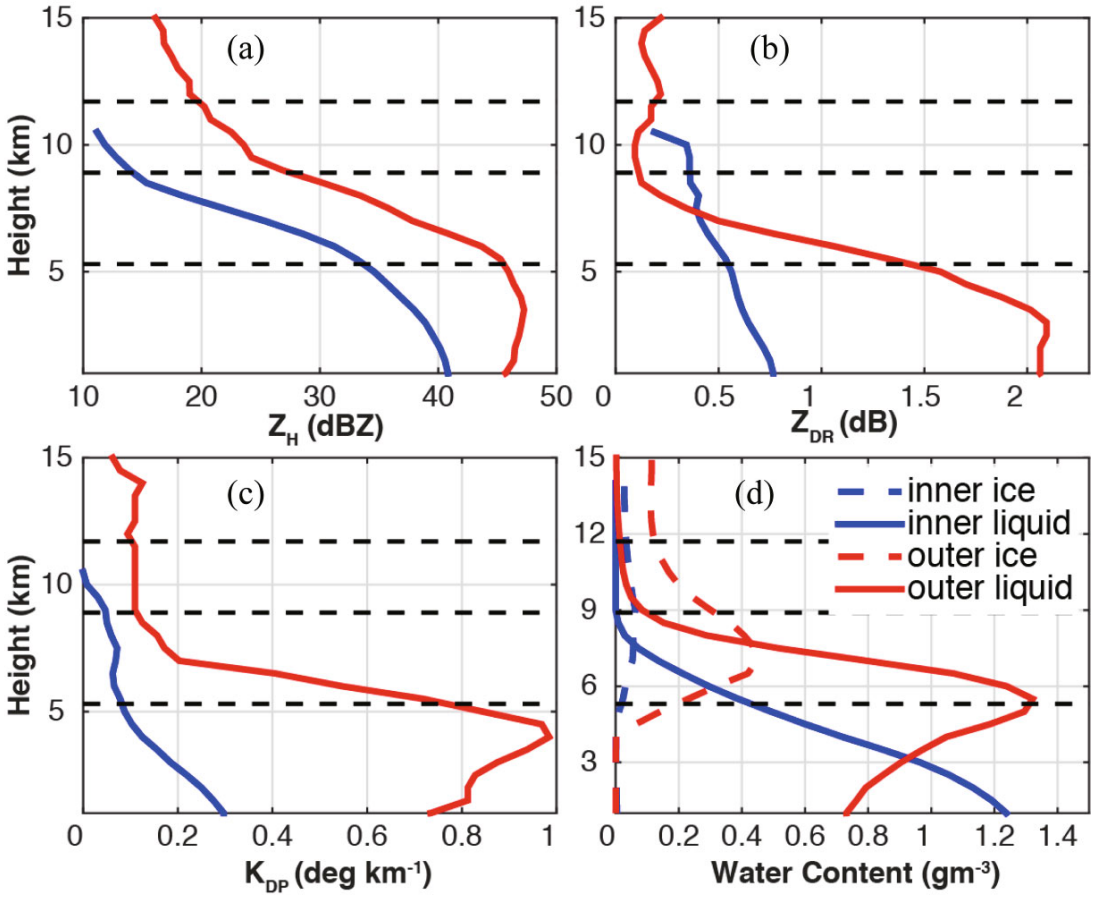


**Fig. 8.** Median profiles of (a) reflectivity, (b) $Z_{DR}$, (c) ice water content, and (d) liquid water content at the convective center in the inner rainband (blue lines) and the mature stage of the outer rainband (red lines) of Typhoon Nida (2016). [Reprinted from Wu et al. (2018b). © American Meteorological Society. Used with permission.]

for initialization and assimilating dual-pol radar measurements is urgent for the numerical forecasting of mesoscale weather systems.

Multi-frequency and phased arrays are two emerging technologies that can provide additional microphysical information and reduce the radar sampling time. Phased array dual-pol radars can measure precipitation systems more rapidly, which also gains more dynamical and microphysical information. However, the H- and V-polarized beam matching off the broadside affecting the dual-pol measurement remains a challenge for radar engineers. In contrast, the system of multi-frequency dual-pol radars is based on the variations of the Mie scattering effect with respect to the frequency of electromagnetic waves, which also provides information on the sizes of hydrometeors. It is anticipated that these two types of technologies will mature in the next decade and make significant impacts in the future of radar meteorology.

***Acknowledgements.*** This work was primarily supported by the National Key Research and Development Program of China (Grant Nos. 2017YFC1501703 and 2018YFC1506404), the National Natural Science Foundation of China (Grant Nos. 41875053, 41475015 and 41322032), the National Fundamental Research 973 Program of China (Grant Nos. 2013CB430101 and 2015CB452800), the Open Research Program of the State Key Laboratory of Severe Weather, and the Key Research Development Program of Jiangsu Science and Technology Department (Social Development Program, No. BE2016732).

## REFERENCES

Barnes, H. C., and R. A. Houze Jr., 2016: Comparison of observed and simulated spatial patterns of ice microphysical processes in tropical oceanic mesoscale convective systems. *J. Geophys. Res.*, **121**, 8269–8296, https://doi.org/10.1002/2016JD025074.

Blanchard, D. C., 1953: Raindrop size-distribution in hawaiian rains. *J. Meteor.*, **10**, 457–473, https://doi.org/10.1175/1520-0469(1953)010<0457:RSDIHR>2.0.CO;2.

Bluestein, H. B., and Coauthors, 2014: Radar in atmospheric sciences and related research: Current systems, emerging technology, and future needs. *Bull. Amer. Meteor. Soc.*, **95**, 1850–1861, https://doi.org/10.1175/BAMS-D-13-00079.1.

Bringi, V. N., and V. Chandrasekar, 2001: *Polarimetric Doppler Weather Radar*: *Principles and Applications*. Cambridge University Press, 664 pp.

Bringi, V. N., V. Chandrasekar, N. Balakrishnan, and D. S. Zrnic, 1990: An examination of propagation effects in rainfall

on radar measurements at microwave frequencies. *J. Atmos. Oceanic Technol.*, **7**, 829–840, https://doi.org/10.1175/1520-0426(1990)007<0829:AEOPEI>2.0.CO;2.

Bringi, V. N., V. Chandrasekar, J. Hubbert, E. Gorgucci, W. L. Randeu, and M. Schoenhuber, 2003: Raindrop size distribution in different climatic regimes from disdrometer and dual-polarized radar analysis. *J. Atmos. Sci.*, **60**, 354–365, https://doi.org/10.1175/1520-0469(2003)060<0354:RSDIDC>2.0.CO;2.

Bringi, V. N., M. A. Rico-Ramirez, and M. Thurai, 2011: Rainfall estimation with an operational polarimetric C-band radar in the united kingdom: Comparison with a gauge network and error analysis. *Journal of Hydrometeorology*, **12**, 935–954, https://doi.org/10.1175/JHM-D-10-05013.1.

Carey, L. D., S. A. Rutledge, D. A. Ahijevych, and T. D. Keenan, 2000: Correcting propagation effects in C-band polarimetric radar observations of tropical convection using differential propagation phase. *J. Appl. Meteor.*, **39**, 1405–1433, https://doi.org/10.1175/1520-0450(2000)039<1405:CPEICB>2.0.CO;2.

Chandrasekar, V., L. Baldini, N. Bharadwaj, and P. L. Smith, 2015: Calibration procedures for global precipitation-measurement ground-validation radars. *URSI Radio Science Bulletin*, **355**, 45–73, https://doi.org/10.23919/URSIRSB.2015.7909473.

Chang, W.-Y., T.-C. C. Wang, and P.-L. Lin, 2009: Characteristics of the raindrop size distribution and drop shape relation in typhoon systems in the western pacific from the 2D video disdrometer and NCU C-band polarimetric radar. *J. Atmos. Oceanic Technol.*, **26**, 1973–1993, https://doi.org/10.1175/2009JTECHA1236.1.

Chen, C., H. Xiao, L. Feng, Z.-F. Li, and J.-J. Zhou, 2014: A dual-polarimetric analysis of a strong hailstorm in Beijing. *Journal of Anhui Agricultural Sciences*, **42**, 7511–7515, 7536, https://doi.org/10.3969/j.issn.0517-6611.2014.22.076. (in Chinese with English abstract)

Chen, C., Z.-Q. Hu, S. Hu, and Y. Zhang, 2018: Preliminary analysis of data quality of guangzhou s-band polarimetric weather radar. *Journal of Tropical Meteorology*, **34**, 59–67, https://doi.org/10.16032/j.issn.1004-4965.2018.01.006. (in Chinese with English abstract)

Chen, G., and Coauthors, 2017: Improving polarimetric C-band radar rainfall estimation with two-dimensional video disdrometer observations in eastern China. *Journal of Hydrometeorology*, **18**, 1375–1391, https://doi.org/10.1175/JHM-D-16-0215.1.

Dolan, B., S. A. Rutledge, S. Lim, V. Chandrasekar, and M. Thurai, 2013: A robust C-band hydrometeor identification algorithm and application to a long-term polarimetric radar dataset. *Journal of Applied Meteorology and Climatology*, **52**, 2162–2186, https://doi.org/10.1175/JAMC-D-12-0275.1.

Dolan, B., B. Fuchs, S. A. Rutledge, E. A. Barnes, and E. J. Thompson, 2018: Primary modes of global drop size distributions. *J. Atmos. Sci.*, **75**, 1453–1476, https://doi.org/10.1175/JAS-D-17-0242.1.

Doviak, R. J., and D. S. Zrnić, 1993: *Doppler Radar and Weather Observations*. 2nd ed., Dover Publications, 562 pp.

Du, M. Y., L. P. Liu, Z. Q. Hu, and R. Yu, 2012: Quality control of differential propagation phase shift for dual linear polarization radar. *Journal of Applied Meteorological Science*, **23**, 710–720, https://doi.org/10.3969/j.issn.1001-7313.2012.06.008. (in Chinese with English abstract)

Du, M.-Y., L.-P. Liu, and Z.-Q. Hu, 2013: System bias calibration of differential reflectivity for dual linear polarization radar. *Plateau Meteorology*, **32**, 1174–1185. (in Chinese with English abstract)

Feng, L., H. Xiao, and Y. Sun, 2018: A study on hydrometeor classification and application based on X-band dual-polarization radar measurements. *Climatic and Environmental Research*, **23**, 366–386. (in Chinese with English abstract)

Gao, W. H., C.-H. Sui, J. W. Fan, Z. Q. Hu, and L. Z. Zhong, 2016: A study of cloud microphysics and precipitation over the Tibetan Plateau by radar observations and cloud-resolving model simulations. *J. Geophys. Res.*, **121**, 13 735–13 752, https://doi.org/10.1002/2015JD024196.

Gao, Y.-F., Y.-D. Chen, G. David, I. Kyoko, and J.-Y. Ye, 2014: Analysis of JPOLE algorithm with a dual polarization radar in different precipitation processes. *Journal of Tropical Meteorology*, **30**, 361–367, https://doi.org/10.3969/j.issn.1004-4965.2014.02.017. (in Chinese with English abstract)

Giangrande, S. E., R. McGraw, and L. Lei, 2013: An Application of Linear Programming to Polarimetric Radar Differential Phase Processing. *Journal of Atmospheric and Oceanic Technology*, **30**, 1716–1729.

Gorgucci, E., G. Scarchilli, and V. Chandrasekar, 1992: Calibration of radars using polarimetric techniques. *IEEE Trans. Geosci. Remote Sens.*, **30**, 853–858, https://doi.org/10.1109/36.175319.

Gorgucci, E., G. Scarchilli, V. Chandrasekar, and V. N. Bringi, 2001: Rainfall estimation from polarimetric radar measurements: Composite algorithms immune to variability in raindrop shape–size relation. *J. Atmos. Oceanic Technol.*, **18**, 1773–1786, https://doi.org/10.1175/1520-0426(2001)018<1773:REFPRM>2.0.CO;2.

Gu, J., Y.-J. Zhou, Z. Shi, and L. Huang, 2015: The evolution characteristic of hydrometeor in a thunderstorm. *Journal of Chengdu University of Information Technology*, **30**, 505–511, https://doi.org/10.3969/j.issn.1671-1742.2015.05.016. (in Chinese with English abstract)

Hu, H. F., D. R. Chen, Z. G. Chu, and X. K. Wang, 2018: Effect of rotary joints of dual-polarization weather radar on zdr measurements. *Meteorological Science and Technology*, **46**, 429–435, https://doi.org/10.19517/j.1671-6345.20170310. (in Chinese with English abstract)

Hu, Z. Q., and L. P. Liu, 2014: Applications of wavelet analysis in differential propagation phase shift data de-noising. *Adv. Atmos. Sci.*, **31**, 825–835, https://doi.org/10.1007/s00376-013-3095-y.

Hu, Z. Q., L. P. Liu, and L. L. Wu, 2014: Comparison among several system biases calibration methods on C-band polarimetric radar. *Plateau Meteorology*, **33**, 221–231. (in Chinese with English abstract)

Huang, H., 2018: A research on optimization-based rainfall parameter retrieval using polarimetric radar data. PhD dissertation, Nanjing University, 178 pp. (in Chinese with English abstract)

Huang, H., G. F. Zhang, K. Zhao, and S. E. Giangrande, 2017: A hybrid method to estimate specific differential phase and rainfall with linear programming and physics constraints. *IEEE Trans. Geosci. Remote Sens.*, **55**, 96–111, https://doi.org/10.1109/TGRS.2016.2596295.

Huang, H., and Coauthors, 2018a: Quantitative precipitation estimation with operational polarimetric radar measurements in southern china: A differential phase–based variational approach. *J. Atmos. Oceanic Technol.*, **35**, 1253–1271, https://

doi.org/10.1175/JTECH-D-17-0142.1.

Huang, H., G. F. Zhang, K. Zhao, S. Liu, L. Wen, G. Chen, and Z. W. Yang, 2019: Uncertainty in retrieving raindrop size distribution from polarimetric radar measurements. *J. Atmos. Oceanic Technol*., **36**, 585–605, https://doi.org/10.1175/JTECH-D-18-0107.1.

Huang, X. Y., L. Zhang, X. Lu, Y. Y. Li, J. N. Yin, L. Ma, and S. Zhang, 2018b: Attenuation correction for C-band dual-polarization radar reflectivity factor and the accuracy improvement of precipitation estimation. *Journal of the Meteorological Sciences*, **38**, 237–246. (in Chinese with English abstract)

Hubbert, J., and V. N. Bringi, 1995: An iterative filtering technique for the analysis of copolar differential phase and dual-frequency radar measurements. *J. Atmos. Oceanic Technol.*, **12**, 643–648, https://doi.org/10.1175/1520-0426(1995)012<0643:AIFTFT>2.0.CO;2.

Hubbert, J., V. Chandrasekar, V. N. Bringi, and P. Meischner, 1993: Processing and interpretation of coherent dual-polarized radar measurements. *J. Atmos. Oceanic Technol.*, **10**, 155–164, https://doi.org/10.1175/1520-0426(1993)010<0155:PAIOCD>2.0.CO;2.

Hubbert, J. C., V. N. Bringi, and D. Brunkow, 2003: Studies of the polarimetric covariance matrix. Part I: Calibration methodology. *J. Atmos. Oceanic Technol.*, **20**, 696–706, https://doi.org/10.1175/1520-0426(2003)20<696:SOTPCM>2.0.CO;2.

Hubbert, J. C., J. W. Wilson, T. M. Weckwerth, S. M. Ellis, M. Dixon, and E. Loew, 2018: S-pol's polarimetric data reveal detailed storm features (and insect behavior). *Bull. Amer. Meteor. Soc.*, **99**, 2045–2060, https://doi.org/10.1175/BAMS-D-17-0317.1.

Jung, Y., G. F. Zhang, and M. Xue, 2008: Assimilation of simulated polarimetric radar data for a convective storm using the ensemble kalman filter. Part I: Observation operators for reflectivity and polarimetric variables. *Mon. Wea. Rev.*, **136**, 2228–2245, https://doi.org/10.1175/2007MWR2083.1.

Kumjian, M. R., 2013: Principles and applications of dual-polarization weather radar. Part I: Description of the polarimetric radar variables. *Journal of Operational Meteorology*, **1**, 226–242, https://doi.org/10.15191/nwajom.2013.0119.

Kumjian, M. R., and A. V. Ryzhkov, 2008: Polarimetric signatures in supercell thunderstorms. *Journal of Applied Meteorology and Climatology*, **47**, 1940–1961, https://doi.org/10.1175/2007JAMC1874.1.

Kumjian, M. R., and A. V. Ryzhkov, 2010: The impact of evaporation on polarimetric characteristics of rain: Theoretical model and practical implications. *Journal of Applied Meteorology and Climatology*, **49**, 1247–1267, https://doi.org/10.1175/2010JAMC2243.1.

Kumjian, M. R., and A. V. Ryzhkov, 2012: The impact of size sorting on the polarimetric radar variables. *J. Atmos. Sci.*, **69**, 2042–2060, https://doi.org/10.1175/JAS-D-11-0125.1.

Kumjian, M. R., and O. P. Prat, 2014: The impact of raindrop collisional processes on the polarimetric radar variables. *J. Atmos. Sci.*, **71**, 3052–3067, https://doi.org/10.1175/JAS-D-13-0357.1.

Lee, G. W., 2006: Sources of errors in rainfall measurements by polarimetric radar: Variability of drop size distributions, observational noise, and variation of relationships between R and polarimetric parameters. *J. Atmos. Oceanic Technol.*, **23**, 1005–1028, https://doi.org/10.1175/JTECH1899.1.

Lei, Y.-H., 2014: Attenuation correction of reflectivity factor for X-band dual-polarization radar. *Journal of Chengdu University of Information Technology*, **29**, 586–589, https://doi.org/10.3969/j.issn.1671-1742.2014.06.004. (in Chinese with English abstract)

Li, Z. F., H. Xiao, Z. D. Yao, and L. Feng, 2015: Retrieval of raindrop size distribution by X-band dual-polarization radar. *Climatic and Environmental Research*, **20**, 285–295, https://doi.org/10.3878/j.issn.1006-9585.2014.14021. (in Chinese with English abstract)

Liu, X. T., Q. L. Wan, H. Wang, H. Xiao, Y. Zhang, T. F. Zheng, and L. Feng, 2018: Raindrop size distribution parameters retrieved from guangzhou S-band polarimetric radar observations. *Journal of Meteorological Research*, **32**, 571–583, https://doi.org/10.1007/s13351-018-7152-4.

Luo, Y. L., and Coauthors, 2017: The southern China monsoon rainfall experiment (SCMREX). *Bull. Amer. Meteor. Soc.*, **98**, 999–1013, https://doi.org/10.1175/BAMS-D-15-00235.1.

Marzano, F. S., D. Scaranari, M. Montopoli, and G. Vulpiani, 2008: Supervised classification and estimation of hydrometeors from C-band dual-polarized radars: A bayesian approach. *IEEE Trans. Geosci. Remote Sens.*, **46**, 85–98, https://doi.org/10.1109/TGRS.2007.906476.

Mei, Y., Z. Q. Hu, X. Y. Huang, and C. Chen, 2018: A study of convective clouds in the Tibetan Plateau based on dual polarimetric radar observations. *Acta Meteorologica Sinica*, **76**, 1014–1028, http://doi.org/10.11676/qxxb2018.037. (in Chinese with English abstract)

Park, H. S., A. V. Ryzhkov, D. S. Zrnić, and K.-E. Kim, 2009: The hydrometeor classification algorithm for the polarimetric WSR-88D: Description and application to an MCS. *Wea. Forecasting*, **24**, 730–748, https://doi.org/10.1175/2008WAF2222205.1.

Petersen, W. A., and S. A. Rutledge, 2001: Regional variability in tropical convection: Observations from TRMM. *J. Climate*, **14**, 3566–3586, https://doi.org/10.1175/1520-0442(2001)014<3566:RVITCO>2.0.CO;2.

Posselt, D. J., X. L. Li, S. A. Tushaus, and J. R. Mecikalski, 2015: Assimilation of dual-polarization radar observations in mixed- and ice-phase regions of convective storms: Information content and forward model errors. *Mon. Wea. Rev.*, **143**, 2611–2636, https://doi.org/10.1175/MWR-D-14-00347.1.

Ran, Y.-B., M. Sun, M.-Q. Gao, and H.-J. Wang, 2017: Study on hydrometeor identification based on deep learning. *Journal of Chengdu University of Information Technology*, **32**, 590–596, https://doi.org/10.16836/j.cnki.jcuit.2017.06.003. (in Chinese with English abstract)

Ryzhkov, A., M. Pinsky, A. Pokrovsky, and A. Khain, 2011: Polarimetric radar observation operator for a cloud model with spectral microphysics. *Journal of Applied Meteorology and Climatology*, **50**, 873–894, https://doi.org/10.1175/2010JAMC2363.1.

Ryzhkov, A. V., and D. Zrnić, 1995: Comparison of dual-polarization radar estimators of rain. *J. Atmos. Oceanic Technol.*, **12**, 249–256, https://doi.org/10.1175/1520-0426(1995)012<0249:CODPRE>2.0.CO;2.

Ryzhkov, A. V., S. E. Giangrande, and T. J. Schuur, 2005a: Rainfall estimation with a polarimetric prototype of WSR-88D. *J. Appl. Meteor.*, **44**, 502–515, https://doi.org/10.1175/JAM2213.1.

Ryzhkov, A. V., S. E. Giangrande, V. M. Melnikov, and T. J. Schuur, 2005b: Calibration issues of dual-polarization radar measurements. *J. Atmos. Oceanic Technol.*, **22**, 1138–1155,

https://doi.org/10.1175/JTECH1772.1.

Seliga, T. A., and V. N. Bringi, 1976: Potential use of radar differential reflectivity measurements at orthogonal polarizations for measuring precipitation. *J. Appl. Meteor.*, **15**, 69–76, https://doi.org/10.1175/1520-0450(1976)015<0069:PUORDR>2.0.CO;2.

Seliga, T. A., and V. N. Bringi, 1978: Differential reflectivity and differential phase shift: Applications in radar meteorology. *Radio Sci.*, **13**, 271–275, https://doi.org/10.1029/RS013i002p00271.

Sun, Y., H. Xiao, L. Feng, H.-L. Yang, C. Chen, and Y.-J. Zhou, 2015: A new method for the quality control of differential propagation phase shift for dual-polarization radar: The linear fitting and recurrence method. *Journal of Chengdu University of Information Technology*, **30**, 421–427, https://doi.org/10.3969/j.issn.1671-1742.2015.05.003. (in Chinese with English abstract)

Testud, J., E. Le Bouar, E. Obligis, and M. Ali-Mehenni, 2000: The rain profiling algorithm applied to polarimetric weather radar. *J. Atmos. Oceanic Technol.*, **17**, 332–356, https://doi.org/10.1175/1520-0426(2000)017<0332:TRPAAT>2.0.CO;2.

Ulbrich, C. W., 1983: Natural variations in the analytical form of the raindrop size distribution. *J. Climate Appl. Meteor.*, **22**, 1764–1775, https://doi.org/10.1175/1520-0450(1983)022<1764:NVITAF>2.0.CO;2.

Vivekanandan, J., W. M. Adams, and V. N. Bringi, 1991: Rigorous approach to polarimetric radar modeling of hydrometeor orientation distributions. *J. Appl. Meteor.*, **30**, 1053–1063, https://doi.org/10.1175/1520-0450(1991)030<1053:RATPRM>2.0.CO;2.

Vivekanandan, J., D. S. Zrnic, S. M. Ellis, R. Oye, A. V. Ryzhkov, and J. Straka, 1999: Cloud microphysics retrieval using S-band dual-polarization radar measurements. *Bull. Amer. Meteor. Soc.*, **80**, 381–388, https://doi.org/10.1175/1520-0477(1999)080<0381:CMRUSB>2.0.CO;2.

Vivekanandan, J., G. F. Zhang, S. M. Ellis, D. Rajopadhyaya, and S. K. Avery, 2003: Radar reflectivity calibration using differential propagation phase measurement. *Radio Sci.*, **38**, 8049, https://doi.org/10.1029/2002RS002676.

Wang, H., Q. L. Wan, J. F. Yin, and W. Y. Ding, 2016a: Application of the dual-polarization radar data in numerical modeling studies: Construction of the simulator. *Acta Meteorologica Sinica*, **74**, 229–243, http://dx.doi.org/10.11676/qxxb2016.017. (in Chinese with English abstract)

Wang, H., N. G. Wu, Q. L. Wan, and T. Zhan, 2018a: Analysis of s-band polarimetric radar observations of a hail-producing supercell. *Acta Meteorologica Sinica*, **76**, 92–103, http://dx.doi.org/10.11676/qxxb2017.078.

Wang, H., F. Kong, N. Wu, H. Lan, and J. Yin, 2019: An investigation into microphysical structure of a squall line in South China observed with a polarimetric radar and a disdrometer. *Atmospheric Research*, **226**, 171-180, https://doi.org/10.1016/j.atmosres.2019.04.009.

Wang, M. J., K. Zhao, M. Xue, G. F. Zhang, S. Liu, L. Wen, and G. Chen, 2016b: Precipitation microphysics characteristics of a Typhoon Matmo (2014) rainband after landfall over eastern China based on polarimetric radar observations. *J. Geophys. Res.*, **121**, 12 415–12 433, https://doi.org/10.1002/2016JD025307.

Wang, M. J., K. Zhao, W.-C. Lee, and F. Q. Zhang, 2018b: Microphysical and kinematic structure of convective-scale elements in the inner rainband of typhoon matmo (2014) after landfall. *J. Geophys. Res.*, **123**, 6549–6564, https://doi.org/10.1029/2018JD028578.

Wang, Y., 2018: Understanding and prediction of rainfall associated with landfalling tropical cyclones (UPDRAFT). *Proceedings of 20th EGU General Assembly*, 4–13 April 2018, Vienna, Austria, p.2916.

Wang, Y. T., and V. Chandrasekar, 2009: Algorithm for estimation of the specific differential phase. *J. Atmos. Oceanic Technol.*, **26**, 2565–2578, https://doi.org/10.1175/2009JTECHA1358.1.

Wei, Q., Z.-Q. Hu, and L.-P. Liu, 2014: Comparative analysis of five filtering methods of differential propagation phase shift for polarization radar subtitle as needed. *Journal of Chengdu University of Information Technology*, **29**, 596–602, https://doi.org/10.3969/j.issn.1671-1742.2014.06.006. (in Chinese with English abstract)

Wei, Q., Z. Q. Hu, L. P. Liu, and L. L. Wu, 2016: C-band polarization radar data preprocessing and its application to rainfall estimation. *Plateau Meteorology*, **35**, 231–243. (in Chinese with English abstract)

Wen, G., A. Protat, P. T. May, X. Z. Wang, and W. Moran, 2015: A cluster-based method for hydrometeor classification using polarimetric variables. Part I: Interpretation and analysis. *J. Atmos. Oceanic Technol.*, **32**, 1320–1340, https://doi.org/10.1175/JTECH-D-13-00178.1.

Wen, G., A. Protat, P. T. May, W. Moran, and M. Dixon, 2016: A cluster-based method for hydrometeor classification using polarimetric variables. Part II: Classification. *J. Atmos. Oceanic Technol.*, **33**, 45–60, https://doi.org/10.1175/JTECH-D-14-00084.1.

Wen, J., 2017: Observing and simulating the microphysial structure of a subtropical squall line in Eastern China. Nanjing University, 72 pp. (in Chinese)

Wen, J., and Coauthors, 2017: Evolution of microphysical structure of a subtropical squall line observed by a polarimetric radar and a disdrometer during OPACC in Eastern China. *J. Geophys. Res.*, **122**, 8033–8050, https://doi.org/10.1002/2016JD026346.

Wen, L., and Coauthors, 2018: Drop size distribution characteristics of seven typhoons in China. *J. Geophys. Res.*, **123**, 6529–6548, https://doi.org/10.1029/2017JD027950.

Wu, C., L. P. Liu, M. Wei, B. Z. Xi, and M. H. Yu, 2018a: Statistics-based optimization of the polarimetric radar hydrometeor classification algorithm and its application for a squall line in South China. *Adv. Atmos. Sci.*, **35**, 296–316, https://doi.org/10.1007/s00376-017-6241-0.

Wu, D., and Coauthors, 2018b: Kinematics and microphysics of convection in the outer rainband of typhoon nida (2016) revealed by polarimetric radar. *Mon. Wea. Rev.*, **146**, 2147–2159, https://doi.org/10.1175/MWR-D-17-0320.1.

Wu, H., and X. Y. Huang, 2014: Schemes for attenuation correction of radar reflectivity factor, ground clutter discrimination and compensation of a X-band dual-polarization radar. *Journal of the Meteorological Sciences*, **34**, 32–38, https://doi.org/10.3969/2012jms.0183. (in Chinese with English abstract)

Wu, W., Y.-J. Zhou, X.-M. Li, and L. Zhai, 2017: Comparative study on quality control methods of X-band dual-polarization radar data. *Journal of Chengdu University of Information Technology*, **32**, 19–27, https://doi.org/10.16836/j.cnki.jcuit.2017.01.004. (in Chinese with English abstract)

Xue, M., 2016: Preface to the special issue on the "observa-

tion, prediction and analysis of severe convection of China" (OPACC) national "973" project. *Adv. Atmos. Sci.*, **33**, 1099–1101, https://doi.org/10.1007/s00376-016-0002-3.

Yang, J., K. Zhao, and G. Zhang, 2017: A bayesian hydrometeor classification algorithm for C-band polarimetric radar. *Proc. 38th Conf. on Radar Meteorology*.

Zhang, G. F., 2016: *Weather Radar Polarimetry*. CRC Press, 322 pp.

Zhang, G., J. Vivekanandan, and E. Brandes, 2001: A method for estimating rain rate and drop size distribution from polarimetric radar measurements. *IEEE Trans. Geosci. Remote Sens.*, **39**, 830–841, https://doi.org/10.1109/36.917906.

Zhang, G. F., and Coauthors, 2019: Current status and future challenges of weather radar polarimetry: Bridging the gap between radar meteorology/hydrology/engineering and numerical weather prediction. *Adv. Atmos. Sci.* **36**, 571–588, https://doi.org/10.1007/s00376-019-8172-4.

Zhang, J. Y., C. A. Zhang, Y. Ge, and J. J. Zhu, 2018: Characteristics of x-band dual-polarization doppler radar products during strong tornado around typhoon mujigae in foshan. *Meteorological Science and Technology*, **46**, 163–169, https://doi.org/10.19517/j.1671-6345.20170094. (in Chinese with English abstract)

Zhang, X.-T., W.-T. Li, Y. Peng, and M.-X. Yin, 2017a: Analysis of the characteristics of polarimetric weather radar for a super-cell hail in Qingyuan. *Guangdong Meteorology*, **39**, 41–44, 51, https://doi.org/10.3969/j.issn.1007-6190.2017.04.010. (in Chinese with English abstract)

Zhang, Y., D.-M. Hu, and H.-Y. Li, 2017b: Preliminary application of a dual polarization weather radar in guangzhou during a short-range intensive rain. *Guangdong Meteorology*, **39**, 26–29, https://doi.org/10.3969/j.issn.1007-6190.2017.02.006. (in Chinese with English abstract)

Zhang, Y., C.-C. Tian, and C. Luo, 2017c: Preliminary analysis of quantitative precipitation estimation using Guangzhou dual-polarization weather radar. *Guangdong Meteorology*, **39**, 73–76, https://doi.org/10.3969/j.issn.1007-6190.2017.03.018. (in Chinese)

Zhao, P., and Coauthors, 2018: The third atmospheric scientific experiment for understanding the earth–atmosphere coupled system over the tibetan plateau and its effects. *Bull. Amer. Meteor. Soc.*, **99**, 757–776, https://doi.org/10.1175/BAMS-D-16-0050.1.

Zheng, J. F., J. Zhang, K. Y. Zhu, X. Q. Gao, and T. Zhang, 2014: Analysis of dual polarization weather radar rainfall measuring errors and hydrometeor identification. *Meteorological Science and Technology*, **42**, 364–372, https://doi.org/10.3969/j.issn.1671-6345.2014.03.002. (in Chinese with English abstract)

Zrnic, D. S., V. M. Melnikov, and J. K. Carter, 2006: Calibrating differential reflectivity on the WSR-88D. *J. Atmos. Oceanic Technol.*, **23**, 944–951, https://doi.org/10.1175/JTECH1893.1.

Giangrande, S. E., R. McGraw, and L. Lei, 2013: An Application of Linear Programming to Polarimetric Radar Differential Phase Processing. Journal of Atmospheric and Oceanic Technology, **30**, 1716–1729.